Green Synthesis and Characterization of Zinc Pyridine-2,6-Dicarboxylate Complex and Preparation of Nano-ZnO by Thermal Decomposition

Luo, Huan; Yang, Rong-Gui
School of Materials and Chemistry, Southwest University of Science and Technology, Mianyang 621010, P.R. CHINA

Chen, Zhao-Hui
Department of Basic Science, Rongchang Campus of Southwest University, Chongqing 402460, P.R. CHINA

Zhong, Guo-Qing*[+]
School of Materials and Chemistry, Southwest University of Science and Technology, Mianyang 621010, P.R. CHINA

ABSTRACT: *A complex $[Zn(Hpda)_2]\cdot 2H_2O$ of pyridine-2,6-dicarboxylic acid (H_2pda) was synthesized by a green chemistry approach, namely, room-temperature solid-state reaction. The complex was characterized by elemental analyses, Powder X-Ray Diffraction (PXRD), single crystal X-ray diffraction, Fourier Transform InfraRed (FT-IR) spectroscopy, and ThermoGravimetry and Differential Scanning Calorimetry (TG-DSC). The PXRD result confirmed that the unpurified powder complex was a single phase. The crystal structure of the complex belonged to the monoclinic system with space group $P2_1/c$, and the Zn(II) ion was hexacoordinated by four O atoms and two N atoms. The thermal decomposition of the complex was investigated and the nano-ZnO particles were prepared by pyrolysis of the unpurified powder complex as the precursor. The ZnO particle obtained by pyrolysis at 500 °C was characterized by PXRD and Scanning Electron Microscope (SEM), and its average diameter was about 40 nm.*

KEYWORDS: *Room-temperature solid-state reaction; Pyridine-2,6-dicarboxylic acid; Zn(II) complex; Thermal decomposition; Nanometer zinc oxide.*

INTRODUCTION

It is well known that organic ligand, such as pyridine-carboxyl ligands, plays an important role in the construction of complex [1-10]. The past decade has witnessed explosive development of dicarboxylic acids due to their interesting properties. The aromatic dicarboxylates play an important role in MOF chemistry as the organic backbone liners, and the dicarboxylic acid ligands can chelate with transition or rare earth metal ions to form various

***** *To whom correspondence should be addressed.*
+ E-mail: zgq316@163.com
1021-9986/2022/5/1673-1681 9/$/5.09

complexes in material science [11-14] and biological systems [15-20]. Pyridine-2,6-dicarboxylic acid (H_2pda), a versatile *N*,*O*-donor agent with limited steric hindrance, can display a wide variety of coordination functions. And it has attracted much interest in the synthesis of compounds for its novel topologies and interesting structural motifs.

H_2pda has also become one of the more advantageous ligands for constructing potential pharmacologically active coordination compounds because of its low toxicity and amphophilic nature [21]. The synthesis and characterization of zinc complexes containing pyridine-2,6-dicarboxylates have been reported in many kinds of literature [22-27]. However, they were almost synthesized by liquid phase methods. And these reactions utilized different organic solvents, which may cause environmental pollution. Therefore, the green synthetic method is favorable in these manners. In this study, the Zn(II) complex ($[Zn(Hpda)_2]\cdot 2H_2O$) of pyridine-2,6-dicarboxylic acid was synthesized by room-temperature solid-state reaction [28]. Compared with the liquid phase method, this method is in accord with the requirement of green chemistry, which has the characteristics of simple operation, energy saving, high yield, and less pollution. Then the single crystal was successfully cultured by the solvent evaporation method using the unpurified complex, which confirmed that the powder synthesized by the room-temperature solid-state reaction was a pure phase. There are two ligands in the title complex molecule, both of them lose one proton and retain the other. A complex with a similar structure [29] had been reported. However, this paper focuses on two aspects: a different green chemistry synthesis method and the application of the title complex as a precursor to synthesize nano-ZnO.

ZnO nanoparticles, versatile semiconductors, have become significant materials in recent years because of their novel properties and applications in optoelectronic [30-32]. Many methods for preparing nano-ZnO have been reported such as precipitation, electrodeposition, sol-gel, microemulsion method, and so on [33-37]. These preparation methods involve toxic and hazardous chemicals, which may lead to an environmental crisis. So many thermal decomposition methods use the unpurified complex synthesized by room-temperature solid-state reaction as the precursor is one of the more advantageous methods for synthesizing nano-ZnO. Moreover, the particle size of ZnO, which has a great influence on property and application, can be controlled by adjusting the thermal decomposition temperature within a certain temperature range. In this study, in order to expand the application of the complex, the ZnO particles with high purity and small particle size were obtained by calcination with the title complex as a precursor [38].

EXPERIMENTAL SECTION

Materials and experimental techniques

All reagents were of analytical grade and were used without further purification. Zinc acetate ($Zn(Ac)_2\cdot 2H_2O$), ethanol and disodium ethylenediaminetetraacetate dehydrate (EDTA) were purchased from Sinopharm Chemical Reagent Co., Ltd. (Shanghai, China). Pyridine-2,6-dicarboxylic acid (H_2pda) was obtained from Jinan Henghua Sci. & Tec. Co., Ltd. (Jinan, China).

Elemental analyses for carbon, hydrogen and nitrogen were performed on a Vario EL CUBE instrument (Elementar, Langenselbold, Germany). The contents of zinc in the complex and oxide were determined by EDTA titration. Powder X-ray diffraction measurements were carried out with a D/max-II X-ray diffractometer (Rigaku, Tokyo, Japan) using Cu K_α radiation. FT-IR spectra of a KBr pellet were recorded in the range of 4000–400 cm^{-1} on a Perkin-Elmer Spectrum One spectrometer (PerkinElmer, Waltham, MA, USA). TG-DSC curves were performed by a SDT 650 thermal analyzer (TA Instruments, New Castle, DE, USA), and the measurements were recorded from ambient temperature to 800 °C at a heating rate of 10 °C/min. Crystal determination was performed with a Bruker SMART APEX II CCD diffractometer (Bruker, Karlsruhe, Germany) equipped with a graphite-monochrome-matized Mo K_α radiation (λ = 0.71073 Å). SEM images of particles were measured on a MAIA3 field emission scanning electron microscope system (Tescan, Brno, Czechs).

Synthesis of $[Zn(Hpda)_2]\cdot 2H_2O$

$Zn(Ac)_2\cdot 2H_2O$ (0.220 g, 1.00 mmol) and H_2pda (0.334 g, 2.00 mmol) were mixed up together. The mixture was carefully ground in an agate mortar for 30 min and two drops (approximately 0.1 mL) of ethanol were added as an evocating agent. There was an irritating odor of gas due to acetic acid generation when grinding the mixture, indicating that the reaction did happen. After 4 h,

Table 1: Crystal data and structure refinement parameters of the Zn(II) complex.

Empirical formula	$ZnC_{14}H_{13}O_{10.5}N_2$	Absorption coefficient (mm^{-1})	1.475
Formula weight ($g \cdot mol^{-1}$)	442.63	$F(000)$	900
Temperature (K)	293(2)	Crystal size (mm)	0.28 × 0.26 × 0.23
Crystal system	Monoclinic	Theta range (°)	2.962 to 27.542
Space group	$P2_1/c$	Limiting indices	$-16 \le h \le 18$, $-13 \le k \le 13$, $-17 \le l \le 17$
a (Å)	14.0471(5)	Reflections collected / unique	26636 / 3978 [R(int) = 0.0255]
b (Å)	10.0514(4)	Completeness to theta = 25.242	99.3%
c (Å)	13.7677(5)	Max. and min. transmission	0.7456 and 0.5995
β (°)	116.5820(10)	Goodness-of-fit on F^2	1.062
V ($Å^3$)	1738.42(11)	Final R indices [$I > 2\sigma(I)$]	R_1 = 0.0444, wR_2 = 0.1257
Z	4	R indices (all data)	R_1 = 0.0526, wR_2 = 0.1342
Calculated density ($g \cdot cm^{-3}$)	1.691	Largest diff. peak and hole ($e \cdot Å^{-3}$)	1.739 and − 0.864

there was no pungent-smelling gas produced. The product was white powder and its PXRD pattern was determined. Subsequently, the powder was dissolved with a suitable amount of distilled water, and the filter liquor was heated and concentrated to 30 mL. The colorless crystals of $[Zn(Hpda)_2] \cdot 2.5H_2O$ (which is 0.5 more water molecules then the powder complex) with a yield of about 67% (based on H_2pda) were obtained after 10 days. For the powder complex $ZnC_{14}H_{12}O_{10}N_2$, Anal. Calc. (%): Zn 15.08, C 38.77, H 2.79, N 6.64; Found (%): Zn 14.96, C 38.53, H 2.82, N 6.68. CCDC reference number is 1936767, and the data can be obtained free of charge *via* http://www.ccdc.cam.ac.uk/conts/retrieving.html.

Detailed information about the crystal data and structure refinement parameters of the complex is summarized in Table 1, and the selected bond lengths and angles are listed in Table 2.

Preparation of nano-ZnO

The powder of the title complex was respectively calcined in a muffle furnace at 400, 500, 600, and 800 °C for 30 min, and the nano-ZnO with a narrow size distribution was obtained. The effect of the calcination temperature on the particle size of nano-ZnO was observed.

RESULTS AND DISCUSSION

PXRD analysis

In order to verify the formation of the Zn(II) complex, no further purified powder sample was prepared by the solid-state reaction was measured by powder X-ray diffraction (Fig. 1c). X-ray diffraction data of the samples in the angular range of 2θ = 3–80° were recorded using the D/max-II X-ray diffractometer at room temperature (Cu $K_{\alpha 1}$ radiation, Ni filter, λ = 1.54056 Å, the voltage of 35 kV, current of 60 mA, step width of 2θ = 0.02°, and scanning speed of 8 °·min^{-1}). The strong intensity of the diffraction peaks indicates that the complex has a good crystalline state. The three main strong peaks appear at 2θ = 11.57°, 14.99°, and 21.40° for the complex, and at 2θ = 27.84°, 16.78°, and 19.30° for the ligand pyridine-2,6-dicarboxylic acid (Fig. 1a), while at 2θ = 12.52°, 22.41° and 25.20° for zinc acetate (Fig. 1b). Comparing with the reactants, the strong peak locations of the powder sample are significantly changed, which confirms the formation of the complex [39]. Subsequently, the powder sample of the complex is dissolved in an appropriate amount of distilled water, and the colorless crystals are precipitated after 10 days. In order to check the phase purity of the powder sample, the powder X-ray diffraction of the crystal sample has also been measured and compared (Fig. 1d). As can be seen from the two PXRD patterns, the positions of their diffraction peaks match well, indicating the consistency of the two samples and the high efficiency of the room-temperature solid-state reaction. The "simulation" in Fig. 1e represents the PXRD pattern obtained by simulating powder diffraction with X-ray single crystal diffraction data. Comparing the simulation result with the PXRD pattern of the powder complex, the positions of the diffraction peaks

Table 2: Selected bond lengths (Å) and angles (°) of the Zn(II) complex.

Zn1—N1	2.008(19)	N1—Zn1—O1	79.25(8)	O1—Zn1—O5	94.11(7)
Zn1—N2	2.009(2)	N2—Zn1—O1	113.91(8)	O7—Zn1—O5	152.27(8)
Zn1—O1	2.077(2)	N1—Zn1—O7	104.25(8)	N1—Zn1—O3	73.21(7)
Zn1—O7	2.116(2)	N2—Zn1—O7	78.26(8)	N2—Zn1—O3	93.46(7)
Zn1—O5	2.319(19)	O1—Zn1—O7	97.38(8)	O1—Zn1—O3	152.37(7)
Zn1—O3	2.352(19)	N1—Zn1—O5	102.65(7)	O7—Zn1—O3	91.62(8)
N1—Zn1—N2	166.41(8)	N2—Zn1—O5	74.01(7)	O5—Zn1—O3	89.73(7)

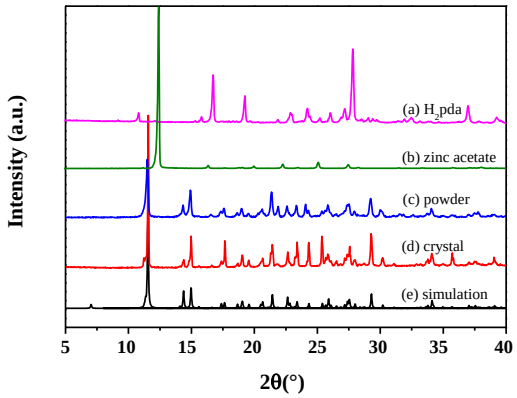

Fig. 1: PXRD patterns of the reactants and the complex [Zn(Hpda)₂]·2H₂O.

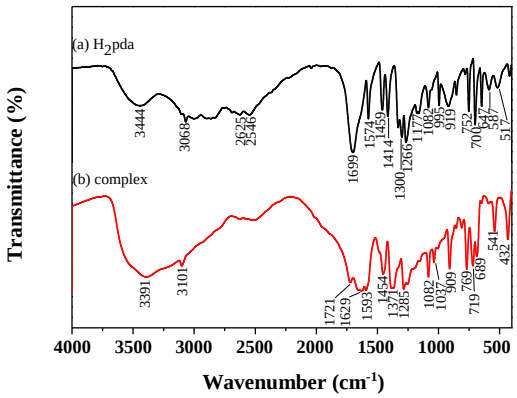

Fig. 2: Infrared spectra of the ligand H₂pda and the powder complex [Zn(Hpda)₂]·2H₂O.

exhibit a slight shift towards higher angles. This may indicate that the crystallization method used to obtain suitable crystals added 0.5 water molecules to the coordination sphere (which proves that there are two water molecules in the powder complex and 2.5 water molecules in the crystal complex).

FT-IR spectra analysis

FT-IR spectra were recorded in the range of 4000–400 cm^{-1} with a resolution of 0.9 cm^{-1} and 40 scans on a Perkin-Elmer Spectrum One spectrometer. FT-IR spectra of H_2pda and the powder complex are shown in Fig. 2. In the high-frequency region, a wide intense absorption band around 3391 cm^{-1} can be assigned to the stretching vibration of the O—H bonds from the water molecules and the ligand $Hpda^-$ anions [40,41], demonstrating the existence of the lattice water molecules in the complex and supporting the molecular formula of the title complex (Fig. 2b). The absorption band at 3101 cm^{-1} is attributed to the stretching vibration of the C—H bonds. The peak at 1593 cm^{-1} is attributed to the C=N bond stretching vibration. The characteristic absorption peak near 1629 cm^{-1} is attributed to the asymmetric stretching vibration of carboxylate group $\nu_{as}(COO^-)$, and this group is also reflected in the FT-IR spectrum by symmetric stretching vibrations of carboxylate group $\nu_s(COO^-)$ at 1371 cm^{-1} [42]. The difference value 258 cm^{-1} between $\nu_{as}(COO^-)$ and $\nu_s(COO^-)$ is larger than 200 cm^{-1}, indicating a monodentate binding of the carboxylate groups to Zn(II) ion [43]. The absorption band at 1454 cm^{-1} can be attributed to the stretching vibration of C=C bonds of the pyridine ring [44]. The presence of bands at 541 and 432 cm^{-1} can be assigned to the stretching vibration of the Zn—N and Zn—O bonds [41]. And these results are also consistent with the results of single crystal structure analysis. The crystal structure shows that the Zn(II) ion is hexacoordinated and bonded to the two N atoms and four O atoms of the two tridentate ligand molecules, which are oriented nearly perpendicular to each other. And the crystal structure of the Zn(II) complex having the molecular formula $[Zn(Hpda)_2]\cdot 2.5H_2O$ with its atom numbering scheme is shown in Fig. 3.

Table 3: Thermal decomposition data of the powder complex [Zn(Hpda)$_2$]·2H$_2$O.

Possible pyrolysis reaction	T_{DSC} (°C)	Mass loss (%)	
		m_{exp}	m_{cal}
{Zn[$C_5H_3N(COOH)(COO)]_2$}·2H_2O			
↓ – 2H_2O	121 (endo.)	8.34	8.31
{Zn[$C_5H_3N(COOH)(COO)]_2$}			
↓ – $C_5H_3N(COOH)_2$	261 (endo.)	38.52	38.54
{Zn[$C_5H_3N(COO)_2$]}			
↓ – C_5H_3N, – CO, – CO_2	531 (exo.)	34.37	34.39
ZnO		18.77	18.76

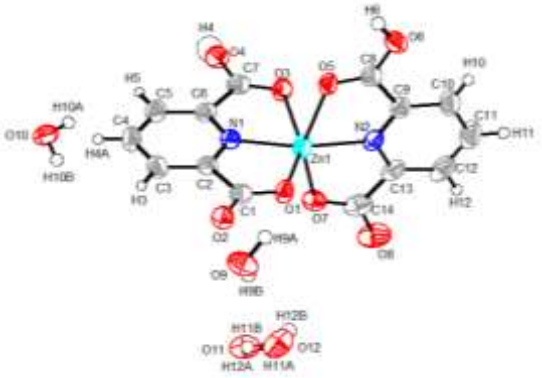

Fig. 3: The molecular structure of the Zn(II) complex.

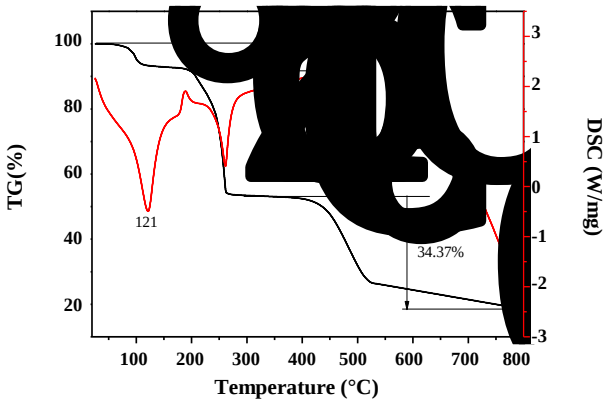

Fig. 4: TG-DSC curves of the complex powder [Zn(Hpda)$_2$]·2H$_2$O.

Thermal analysis

To study the thermal stability of the complex, TG-DSC curves of the powder complex were determined under a nitrogen atmosphere with a heating rate of 10 °C/min. TG-DSC curves of the complex are depicted in Fig. 4. Thermolysis of the synthesized complex is a multistage process. The steps of thermolysis and the solid product are determined from TG-DSC curves, and the intermediate species are verified by mass loss. The thermal analysis reveals that the complex is decomposed through three major processes. The DSC curve shows an endothermic peak at 121 °C. At the same time, the TG curve shows the first mass loss with 8.34% (Calcd. 8.31%), which corresponds very well to the release of two crystal water molecules. And it proves again that there are only two water molecules in the powder complex. There is an endothermic peak at 261 °C corresponding to the second stage mass loss with 38.52% (Calcd. 38.54%), which belongs to the release of an H_2pda ligand molecule (The melting point and boiling point of pyridine-2,6-dicarboxylic acid are 248 °C and 296 °C, respectively). The final stage mass loss is approximately 34.37% (Calcd. 34.39%), owing to the oxidative decomposition of the ligand pda^{2-} anion. The final residue is ZnO with 18.77% (Calcd. 18.76%). And the possible pyrolysis reaction and the experimental and calculated percentage mass losses in the thermal decomposition processes of the Zn(II) complex are summarized in Table 3.

Particle size and morphology of nano-ZnO

The nano-ZnO was prepared by pyrolysis reaction with the unpurified complex as a precursor. Fig. 5 is the PXRD patterns of the pyrolysis products obtained by calcination of the complex at 400, 500, 600, and 800 °C for 0.5 h. As can be seen from Fig. 5, compared with the standard diffraction pattern of zinc oxide (JCPDS No. 36-1451), the pyrolysis products of the complex at 400 °C still have

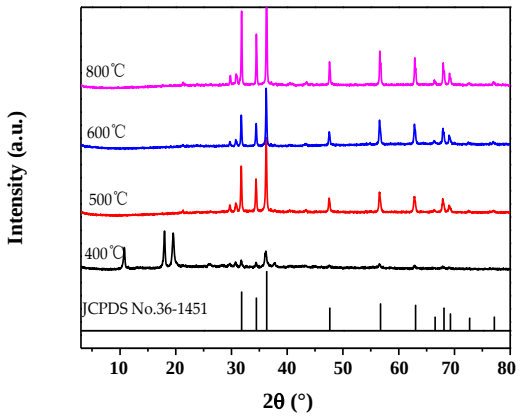

Fig. 5: PXRD patterns obtained by calcination of the powder complex [Zn(Hpda)$_2$]·2H$_2$O at 400, 500, 600, and 800 °C.

some impurity peaks. From this phenomenon, we can conclude that the complex is partially decomposed at this temperature [45]. This is also consistent with the thermal decomposition temperature of the complex. In the range of the nanometer scale, the smaller the grain size is, the wider and weaker the diffraction peaks of the PXRD patterns will be. The diffraction peaks become sharper when the pyrolysis temperature is increased gradually, and this indicates that the grain size of ZnO grows gradually and its crystal shape grows more completely. From the calculation by the X-ray single peak Fourier analysis method [46,47], the average particle diameters of the ZnO products at 400, 500, 600, and 800 °C are 28, 41, 46, and 55 nm, respectively.

Fig. 6 shows the SEM images of the nano-ZnO obtained from calcining the powder complex at 500 °C. As can be seen from Fig. 6, the nano-ZnO particles are almost spherical and uniformly distributed, and its average particle diameter is about 40 nm, which is consistent with the PXRD calculation result. However, due to the absence of a dispersion treatment, there is a certain degree of agglomeration of these nanoparticles, which is also a common phenomenon of nanocrystals. The zinc content in the nano-ZnO is determined by EDTA coordination titration and the result shows that the purity of the nano-ZnO is as high as 99.9%. Therefore, the preparation method of the nano-ZnO has extensive popularization and application value.

CONCLUSIONS

The complex [Zn(Hpda)$_2$]·2H$_2$O was synthesized *via* a room-temperature solid-state reaction, and characterized by EA, PXRD, FT-IR, and TG-DSC. The Zn(II) ion was

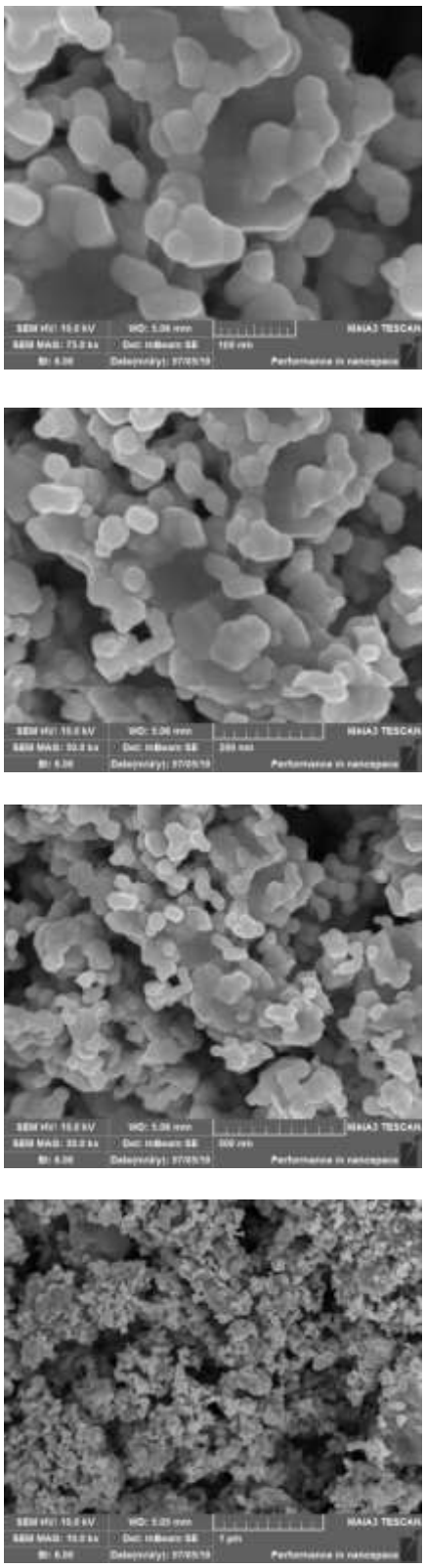

Fig. 6: SEM images of the nano-ZnO.

hexacoordinated by four O atoms and two N atoms from $Hpda^-$ anions. The thermal decomposition of the powder complex mainly included the dehydration process and the oxidative decomposition process of the ligand. The nano-ZnO was prepared by thermal decomposition with the unpurified powder complex as a precursor, and the particle size of zinc oxide gradually grew with the increase of the pyrolysis temperature. The nano-ZnO particle obtained by pyrolysis at 500 °C was spherical, and its average particle diameter was about 40 nm. The particle size of nano-ZnO can be changed by controlling the pyrolysis temperature of the complex precursor. The synthesis method of the Zn(II) complex has the advantages of simple operation, high yield, and environmental friendliness.

Acknowledgments

This research was supported by the Longshan academic talent research supporting program of SWUST (No. 17LZX414).

Received : May. 6, 2021; Accepted : Aug. 7, 2021

REFERENCES

[1] Wang Y.N., Yu J.H., Xu J.Q., Porous Cd^{2+} Supramolecular Network Constructed from 2,3,5,6-Pyridine- tetracarboxylhydrazide, *J. Clust. Sci.*, **29**: 633–639 (2018).

[2] Etaiw S.E.D.H., El-Bendary M.M., Hydrogen Bonded 3D-Network of Silver and 2,6-Pyridinedicarboxylic Acid Complex: Structure and Applications, *J. Mol. Struct.*, **1173**: 7–16 (2018).

[3] Kim D., Kang S.K. Crystal Structure of Aqua-(1*H*-Pyrazole-κN^2) (Pyridine-2,6-Dicarboxylato-κ$^3O^2$,*N*,O^6) Copper(II) Dihydrate, *Acta Crystallogr. E*, **73**: 1875–1877 (2017).

[4] Abdolmaleki S., Ghadermazi M. Novel Pyridinedicarboxamide Derivatives and a Polymeric Copper(II) Complex: Synthesis, Structural Characterization, Electrochemical Behavior, Catalytic and Cytotoxic Studies, *Inorg. Chim. Acta*, **461**: 221–232 (2017).

[5] Dumpala R.M.R., Rawat N., Boda A., Ali S.M., Tomar B.S., Structural, Luminescence, Thermodynamic and Theoretical Studies on Mononuclear Complexes of Eu(III) with Pyridine Monocarboxylate-*N*-Oxides in Aqueous Solution, *Spectrochim. Acta A*, **190**: 150–163 (2018).

[6] Wang H.S., Zhao B., Zhai B., Shi W., Cheng P., Liao D.Z., Yan S.P. Syntheses, Structures, and Photoluminescence of One-Dimensional Lanthanide Coordination Polymers with 2,4,6-Pyridinetricarboxylic Acid, *Cryst. Growth Des.*, **7**: 1851–1857 (2007).

[7] Ye C.R., Zheng J., Li M., Huang X.C., A Zeolite-like MOF Based on a Heterotritopic Linker of Imidazolyl, Carboxyl and Pyridine with a Long-Sought Uks Net on Schwarz′s *D*-Surface, *Chem. Commun.*, **54**: 8769–8772 (2018).

[8] Wang L., Jing G.P., Yang P., Chen J., Two Isostructural Dinuclear Cu^{II} and Co^{II} Complexes with a Multidentate Bridging Ligand 2-(3-(Pyridin-2-yl)-1H-Pyrazol-1-yl)Acetic Acid, *Synth. React. Inorg. Met.-Org. Chem.*, **46(6)**: 799–803 (2016).

[9] Li Z.S., Li X.Y., Liu J.W., He T., Yue K.F., Substituent and Temperature Effect on the Assemblies of Three Lead(II) Coordination Polymers Based on Asymmetrical Biphenyl Tritopic Ligands, *Z. Anorg. Allg. Chem.*, **641(15)**: 2570–2575 (2015).

[10] Li D., Zhong G.Q., Zang Q., Solid–Solid Synthesis, Crystal Structure and Thermal Decomposition of Copper(II) Complex of 2-Picolinic Acid, *Iran. J. Chem. Chem. Eng. (IJCCE)*, **35(4)**: 21−29 (2016).

[11] Li X., Liu A., Du X.D., Wang F.X., Wang C.C., Three Silver Coordination Polymers Constructed from 4,4′-Bipyridine-like Ligands and 2,5-Thiophenedicarboxylic Acid: Crystal Structures and Photocatalytic Performances, *Transit. Metal Chem.*, **44***:* 311–319 (2019).

[12] Xing Y., Liu Y., Xue X., Wang X., Wei L. Copper and Manganese Complexes Based on 1,4-Naphthalene Dicarboxylic Acid Ligand and Its Derivative: Syntheses, Crystal Structures, and Magnetic Properties, *J. Mol. Struct.*, **1154**: 547–556 (2018).

[13] Shi Z., Pan Z., Qin L., Zhou J., Zheng H. Five New Transition Metal Coordination Polymers Based on V-Shaped Bis-triazole Ligand with Aromatic Dicarboxylates: Syntheses, Structures, and Properties, *Cryst. Growth Des.*, **17**: 2757–2766 (2017).

[14] Wang L.D., Tao F., Cheng M.L., Liu Q., Han W., Wu Y.J., Yang D.D., Wang L.J. Syntheses, Crystal Structures, and Luminescence of Two Main-Group Metal Complexes Based on 3,4-Pyrazoledicarboxylic Acid, *J. Coord. Chem.*, **65**: 923–933 (2012).

[15] Siddiqi Z.A., Khalid M., Kumar S., Shahid M., Noor S., Antimicrobial and SOD Activities of Novel Transition Metal Complexes of Pyridine-2,6-Dicarboxylic Acid Containing 4-Picoline as Auxiliary Ligand, *Eur. J. Med. Chem.*, **45**: 264–269 (2010).

[16] Soni K., Singh R.V., Fahmi N., Synthesis of New Macrocyclic Complexes of Transition Metals: Structural Characterization and Biological Activity, *Russ. J. Gen. Chem.*, **87**: 1610–1617 (2017).

[17] Swamy G.Y.S.K., Sivanarayanan P., Sridhar B., Joshi L.R., Crystal Structure Studies and Antimicrobial Activities of Transition Metal Complexes of Pyridine-2,6-Dicarboxylic Acid and Imidazole Containing Water Clusters, *J. Coord. Chem.*, **69**: 1602–1617 (2016).

[18] Mohan G., Nagar R., Agarwal S.C., Mehta K.A., Rao C.S. Syntheses and Anti-inflammatory Activity of Diphenylamine-2,2′-Dicarboxylic Acid and Its Metal Complexes, *J. Enzym. Inhib. Med. Chem.*, **20**: 55–60 (2005).

[19] Sun Y.G., Sun Y.N., You L.X., Liu Y.N., Ding F., Ren B.Y., Xiong G., Dragutan V., Dragutan I. Novel Mononuclear Pt^{2+} and Pd^{2+} Complexes Containing (2,3-f)Pyrazino(1,10)Phenanthroline-2,3-Dicarboxylic Acid as a Multi-Donor Ligand. Synthesis, Structure, Interaction with DNA, in Vitro Cytotoxicity, and Apoptosis, *J. Inorg. Biochem*., **164**: 129–140 (2016).

[20] Zang Q., Zhong G.Q., Wang M.L. A Copper(II) Complex with Pyridine-2,6-Dicarboxylic Acid: Synthesis, Characterization, Thermal Decomposition, Bioactivity and Interactions with Herring Sperm DNA, *Polyhedron*, **100**: 223–230 (2015).

[21] Sakurai H., Kojima Y., Yoshikawa Y., Kawabe K., Yasui H. Antidiabetic Vanadium(IV) and Zinc(II) Complexes, *Coord. Chem. Rev.*, **226**: 187–198 (2002).

[22] Usman M., Khan R.A., Alsalme A., Alharbi W., Alharbi K.H., Jaafar M.H., Khanjer M.A., Tabassum S. Structural, Spectroscopic, and Chemical Bonding Analysis of Zn(II) Complex [Zn(sal)](H_2O): Combined Experimental and Theoretical (NBO, QTAIM, and ELF) Investigation, *Crystals*, **10(4)**: 259 (2020).

[23] Zhang Y.C. Synthesis, Crystal Structure, and Fluorescent Property of a Zn(II) Complex with *N*-Nicotinoylglycine Ligand, *Crystals*, **7(6)**: 151 (2017).

[24] Han L., Jin L., Wang E., Su Z., Synthesis and Characterization of Two Isostructural 3d-4f Coordination Compounds Based on Pyridine-2,6-Dicarboxylic Acid and 4,4′-Bipyridine, *Acta Crystallogr. C*, **75**: 723–727 (2019).

[25] Meng Q., Wang L., Wang D., Yang J., Yue C., Lu J. Synthesis, Crystal Structure, Photoluminescence Properties and Antibacterial Activity of a Zn(II) Coordination Polymer Based on a Paddle-Wheel Clusterhttps, *Crystals*, **7**(4): 112 (2017).

[26] Zhou Y.H. Synthesis, Crystal Structures and Properties of Two Metal–Organic Frameworks Constructed from Pyridine Dicarboxylate and Flexible Bis(imidazole) Ligand, *J. Inorg. Organomet. Polym.*, **23**: 1189–1194 (2013).

[27] Guan Q.L., Liu Z., Wei W.J., Xing Y.H., Liu J., Zhang R., Hou Y.N., Wang X., Bai F.Y. Synthesis, Structure, Spectroscopy of Four Novel Supramolecular Complexes and Cytotoxicity Study by Application of Multiple Parallel Perfused Microbioreactors, *New J. Chem.*, **38**: 3258–3268 (2014).

[28] Zhong G.Q., Jia R.R., Jia Y.Q. Solid-Solid Reaction Preparation for Nanoparticles of Bioinorganic Complex of Bismuth and Serine at Room Temperature, *Adv. Mater. Res.*, **549**: 292–296 (2012).

[29] Okabe N., Oya N. Copper(II) and Zinc(II) Complexes of Pyridine-2,6-Dicarboxylic Acid, *Acta Crystallogr. C*, **56**: 305–307 (2000).

[30] Du Y., Yang Y., Wang X., Li X., Zhou Q., Hydrothermal Synthesis and Optical Properties of CTAB Modified Nano-ZnO, *Integr. Ferroelectr.*, **200(1)**: 161–167 (2019).

[31] Xu Q., Cheng L., Meng L., Wang Z., Bai S., Tian X., Jia X., Qin Y., Flexible Self-Powered ZnO Film UV Sensor with High Response, *ACS Appl. Mater. Inter.*, **11(29)**: 26127–26133 (2019).

[32] Sabonian M., Mahanpoor K., Optimization of Photocatalytic Reduction of Cr(VI) in Water with Nano ZnO/Todorokite as a Catalyst: Using Taguchi Experimental Design, *Iran. J. Chem. Chem. Eng. (IJCCE)*, **38(6)**: 105−113 (2019).

[33] Al-Dahash G., Khilkala W.M., Alwahid S.N.A. Preparation and Characterization of ZnO Nanoparticles by Laser Ablation in NaOH Aqueous Solution, *Iran. J. Chem. Chem. Eng. (IJCCE)*, **37(1)**: 11−16 (2018).

[34] Meng Y., Lin Y., Lin Y., Electrodeposition for the Synthesis of ZnO Nanorods Modified by Surface Attachment with ZnO Nanoparticles and Their Dye-Sensitized Solar Cell Applications, *Ceram. Int.*, **40**: 1693–1698 (2014).

[35] Erol A., Okur S., Comba B., Mermer Ö., Arıkan M.Ç. Humidity Sensing Properties of ZnO Nanoparticles Synthesized by Sol–Gel Process, *Sensor. Actuat. B-Chem.*, **145**: 174–180 (2010).

[36] Inoguchi M., Suzuki K., Kageyama K., Takagi H., Sakabe Y., Monodispersed and Well-Crystallized Zinc Oxide Nanoparticles Fabricated by Microemulsion Method, *J. Am. Ceram. Soc.*, **91(12)**: 3850–3855 (2008).

[37] Fakhari S., Jamzad M., Fard H.K., Green Synthesis of Zinc Oxide Nanoparticles: A Comparison, *Green Chem. Lett. Rev.*, **12**: 19–24 (2019).

[38] Khalaji A.D., Ghorbani M., Dusek M., Eigner V., Nickel(II) and Copper(II) Complexes of a New Tetradentate Schiff Base Ligand: Synthesis, Characterization, Thermal Studies and Use as Precursors for Preparation of NiO and CuO Nanoparticles, *Iran. J. Chem. Chem. Eng. (IJCCE)*, **37(6)**: 27−34 (2018).

[39] Zhong G.Q., Zhong Q. Solid-Solid Synthesis, Characterization, Thermal Decomposition and Antibacterial Activities of Zinc(II) and Nickel(II) Complexes of Glycine-Vanillin Schiff Base Ligand, *Green Chem. Lett. Rev.*, **7**: 236–242 (2014).

[40] Ma X.B., Lin H.L., Zhang J.Y., Zhou X.Z., Han J.C., She Y.X., Qiu C., He Q., Wang J., Rabah T., Preparation and Characterization of Dummy Molecularly Imprinted Polymers for Separation and Determination of Farrerol from *Rhododendron Aganniphum* Using HPLC, *Green Chem. Lett. Rev.*, **11(4)**: 513–522 (2018).

[41] Zhong G.Q., Li D., Zhang Z.-P., Hydrothermal Synthesis, Crystal Structure and Magnetic Property of a Homodinuclear Ternary Coordination Polymer of Nickel(II), *Polyhedron*, **111**: 11–15 (2016).

[42] Gu J.Z., Lv D.Y., Gao Z.Q., Liu J.Z., Dou W., Synthesis, Crystal Structures, and Magnetic Properties of Cobalt(II) and Nickel(II) Complexes of 2,2′-Bipyridine-6,6′-Dicarboxylate: Three Three-Dimensional Networks formed via Hydrogen Bonding Interactions, *Transit. Metal Chem.*, **36(1)**: 53−58 (2011).

[43] Zhong G.Q., Shen J., Jiang Q.Y., Yu K.B., Synthesis and Structural Determination of a Novel Heterometallic Complex $[Sb_2(edta)_2\text{-}\mu_4\text{-}Co(H_2O)_2]\cdot 5.15H_2O$, *Chin. J. Chem.*, **29**: 2650–2654 (2011).

[44] Li Y., Ni B., Li X., Wang X., Zhang D., Zhao Q., Li J., Lu T., Mai W., Pan L., High-Performance Na-Ion Storage of S-Doped Porous Carbon Derived from Conjugated Microporous polymers, *Nano-Micro Lett.*, **11(1)**: 1–13 (2019).

[45] Yang R.G., Wang M.L., Liu T., Zhong G.Q., Room Temperature Solid State Synthesis, Characterization, and Application of a Zinc Complex with Pyromellitic Acid, *Crystals*, **8(2)**: 56 (2018).

[46] Deacon G.B., Phillips R.J., Relationships between the Carbon-Oxygen Stretching Frequencies of Carboxylato Complexes and the Type of Carboxylate Coordination, *Coord. Chem. Rev.*, **33**: 227-250 (1980).

[47] Langford J.I., A Rapid Method for Analysing the Breadths of Diffraction and Spectral Lines Using the Voigt Function, *J. Appl. Crystallogr.*, **11**: 10-14 (1978).